Negative correlation between electrical response and domain size in a Ti-composition-gradient $Pb[(Mg_{1/3}Nb_{2/3})_{1-x}Ti_x]O_3$ crystal near the morphotropic phase boundary

Daisuke Shimizu,[1] Shinya Tsukada,[2] Masato Matsuura,[3] Jun'ya Sakamoto,[1] Seiji Kojima,[4] Kazumichi Namikawa,[5,6] Jun'ichiro Mizuki,[1,6,7] and Kenji Ohwada[1,6,7,*]

[1]*Kwansei Gakuin University, 2-1 Gakuen, Sanda, Hyogo 669-1337, Japan*

[2]*Faculty of Education, Shimane University, Matsue City, Shimane 690-8504, Japan*

[3]*Research Center for Neutron Science and Technology, Comprehensive Research Organization for Science and Society (CROSS), Tokai, Ibaraki 319-1106, Japan*

[4]*Pure and Applied Sciences, University of Tsukuba, Tsukuba City, Ibaraki 305-8573, Japan*

[5]*Tokyo Gakugei University, 4-1-1 Nukuikita-machi, Koganei, Tokyo 184-8501, Japan*

[6]*CREST, Japan Science and Technology Agency (JST), Kawaguchi, Saitama 332-0012, Japan*

[7]*Quantum Beam Science Center (SPring-8), Japan Atomic Energy Agency, 1-1-1 Kouto, Sayo-cho, Sayo-gun, Hyogo 679-5148, Japan*

(Received 12 July 2015; published 30 November 2015)

The phase diagram and the relationship between the crystal coherence length and electrical response of $Pb[(Mg_{1/3}Nb_{2/3})_{1-x}Ti_x]O_3$ (PMN-xPT) near the morphotropic phase boundary (MPB) have been precisely investigated using a single crystal with a Ti composition gradient by synchrotron x-ray diffraction and inelastic light scattering at room temperature. The crystal has two boundaries at Ti compositions of 29.0 and 34.7 mol% which correspond to the phase boundaries between the monoclinic B (M_B) and C (M_C) phases and between the M_C and tetragonal (T) phases, respectively. The crystal coherence length determined from the widths of Bragg peaks varies by over two orders of magnitude in a 10 mol% range of the Ti composition. It is shown that there is a strong negative correlation between the electrical response and the crystal coherence length at the sub-μm scale. The results are explained by the size effects of domains near the MPB.

DOI: 10.1103/PhysRevB.92.174121 PACS number(s): 61.05.C−, 78.35.+c, 77.80.Jk, 77.80.bg

The relaxor ferroelectrics exhibit huge electrical response, i.e., dielectric and piezoelectric coefficients which have broad range temperature dependencies. These properties are useful for various devices, such as condensers, actuators, and transducers, which require a large capacitance/mechanical strain and a small size. One of the most well-known and widely studied relaxor ferroelectrics is $Pb[(Mg_{1/3}Nb_{2/3})_{1-x}Ti_x]O_3$ (PMN-xPT), a solid solution of $Pb(Mg_{1/3}Nb_{2/3})O_3$ (PMN), and $PbTiO_3$ (PT). The x versus temperature phase diagram of PMN-xPT has a ferroelectric rhombohedral (R : $R3m$) Ti-poor region and the ferroelectric tetragonal (T : $P4mm$) Ti-rich region, which are separated by morphotropic phase boundary (MPB: $x \sim 30$ mol%) [Fig. 1(a)]. The MPB is nearly parallel to the temperature axis. PMN-xPT shows maximum electrical response near the MPB composition [1].

Many studies have been devoted to investigating the origin of the large electrical response of relaxor ferroelectrics near the MPB. The observation of stabilized monoclinic symmetry [2–4] is believed to be the most important discovery for relaxor ferroelectrics near the MPB [Fig. 1(a)] [5–8]. Phenomenological [6] and also first-principles [7] calculations have indicated the importance of polarization rotation in the monoclinic symmetries for obtaining large electrical response. As shown in Fig. 1(b), the polarization in the T, R, and O symmetries is aligned in the ⟨001⟩, ⟨111⟩, and ⟨101⟩ directions, respectively. In contrast, the polarization vectors in the monoclinic B (M_B: Cm) and C (M_C: Pm) phases are confined within the (100) and (010) planes, that is, the polarization directions are aligned along $[uvu]$ ($u > v$) and $[u0v]$ ($u < v$), respectively [3,6,7]. This is because the spontaneous polarization vector for the monoclinic symmetry can rotate more easily than that for the R and T symmetries under even a small external field [5,8]. On the other hand, Ishibashi and Iwata explained the large response in a stabilized orthorhombic (O) phase near the MPB by a phenomenological approach [9,10]. They showed that the transverse instability of polarization near the MPB is enhanced without introducing monoclinic phases.

Matsushita *et al.* reported the detailed Ti composition dependence of the dielectric (ε_r at 1 kHz) and the piezoelectric (d_{33}) constants of PMN-xPT which have a sharp peak near 28.0–28.8 mol% and vary by approximately 10%–20% at room temperature even though they have the same Ti composition [Figs. 2(a) and 2(b)] [11]. The origin of the sharp peak and the scattering of the data cannot be understood from the previous phase diagram (averaged symmetry). Matsushita *et al.* predicted that these features of electrical response are related to inhomogeneities in the relaxor ferroelectrics.

Inhomogeneities in the relaxor ferroelectrics have been discussed as a means of explaining the increase in the degree of electrical response by multidomain states [12], the coexistence states of R and T phases [13,14], an adaptive phase that consists of nanodomains [15], the rotation of local polarizations [16], and so forth. Although many experimental results have directly and indirectly shown the existence of inhomogeneities in the relaxor ferroelectrics [17–24], the relationship between the large electrical response and the length scale of the inhomogeneity is not well known.

In this paper, revisiting the precise phase diagram at room temperature, we report the experimental observation of the correlation between the nanometer-to-micrometer inhomogeneity and the large electrical response [11] by synchrotron x-ray diffraction and inelastic light scattering using a single crystal of PMN-xPT with a Ti composition gradient

*ohwada@spring8.or.jp

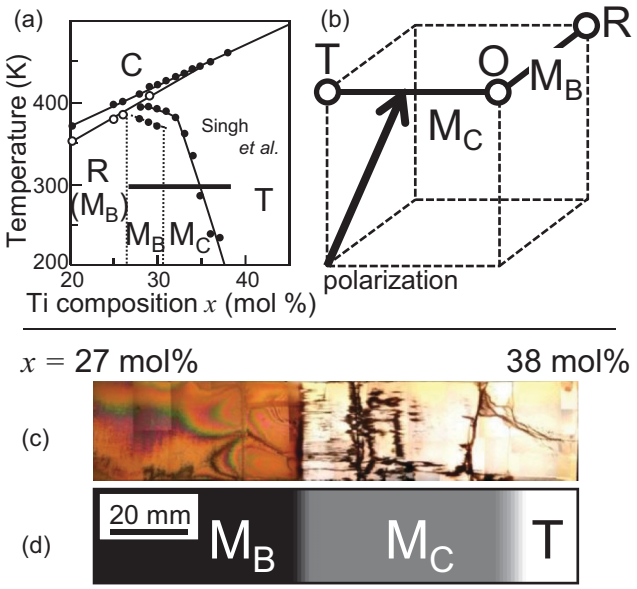

FIG. 1. (Color online) (a) Phase diagram of PMN-xPT obtained by powder x-ray diffraction [28,29]. The thick horizontal line in the phase diagram is the region of our investigation. (b) Crystallographic phases corresponding to different polarization directions [3,7]. (c) Microscopic image of PMN-xPT single crystal with Ti composition gradient. (d) Schematic drawing of the sample.

[Fig. 1(c)]. In the present x-ray measurement, we focus on the Bragg reflection for obtaining the crystal coherence length relating to the inhomogeneity, and we do not focus on the diffuse scattering that originates from nanodomains or polar nanoregions [17,18]. Since the previously proposed phase diagrams of PMN-xPT and $Pb[(Zn_{1/3}Nb_{2/3})_{1-x}Ti_x]O_3$ showed slight differences according to their measurement techniques and conditions, i.e., x-ray or neutron diffraction, powder or single-crystal diffraction [25–27], we employ light scattering to confirm that the bulk of the sample has the same phase boundaries as those observed using x rays.

To gain insight into the origin of the electrical response near the MPB, a systematic study involving the preparation of many samples with slightly different x values is required, considering the x versus temperature phase diagram of PMN-PT [Fig. 1(a)]. As an alternative, a single crystal of PMN-xPT having a Ti composition gradient is ideally suited for this purpose if possible. Fortunately, such a single crystal was provided by JFE Mineral Co., Ltd [11]. By the combination of this crystal with the x-ray microbeams, we can perform precise experiments [30] near the MPB by scanning the x-ray beam relative to the sample position without changing the experimental setup. An as-grown sample was cut to provide a $\{100\}$ plane with dimensions of $62.7^{L} \times 15.0^{W} \times 0.3^{T}$ mm^3, which was optically polished. Figure 1(c) shows a polarized microscopy image of the sample. Two phase boundaries can be clearly observed from the changes in color and brightness. The Ti composition distribution was determined by measurement of the Ti fluorescence (K_α: 4.51 keV) intensities in comparison with reference PMN-xPT ($x = 38.7$ and 0 mol%) samples using a 200×100 μm^2 x-ray beam. We also confirmed that the intensity of the Pb fluorescence (L_β: 12.61 keV) was almost constant at all positions, which was used for the normalization of the measured Ti fluorescence intensities. The Ti composition of the crystal changed from 27.0 to 38.0 mol% over its length of 62.7 mm, while the absolute value of deduced Ti composition had an error of ± 0.6 mol%. By comparison with the previous reports [27–29], we estimated the phase in each region in Fig. 1(c) to be M_B, M_C, and T as shown in Fig. 1(d). The composition range of our measurements is drawn with a thick horizontal line in Fig. 1(a).

The synchrotron x-ray diffraction experiments were performed at BL22XU in SPring-8 [31]. The incident x-ray energy was tuned to 12.94 keV (=0.0958 nm), just below the PbL_{III} absorption edge (13.04 keV). The penetration depth of the x rays in PMN-xPT was estimated to be 14 μm. We mainly focused on the pseudocubic (400) reflection. The size of the incident beam was 200×200 μm^2. The resolution in the reciprocal space along the wave-vector (longitudinal) direction was approximately 0.001 nm^{-1}, corresponding to a crystal coherence length of 1 μm.

The inelastic light scattering in the GHz frequency range was measured using a Fabry-Perot interferometer [32] under a microscope in the backscattering geometry with incident light of $\lambda = 532$ nm. The incident beam was focused to a spot of up to 10 μm diameter.

Figure 3 shows typical peak profiles obtained by x-ray diffraction in the longitudinal direction. The lattice constants as a function of the Ti composition are shown in Fig. 2(c) using solid marks. Two phase boundaries are also clearly indicated from the changes in lattice constants. We also show the results of Singh *et al.* using open marks [28]. Our results are consistent with those in previous reports [27–29], and the two phase boundaries at Ti compositions of 29.0 and 34.7 mol% can be assigned to the M_B–M_C and M_C–T phase boundaries, respectively.

Most of the (400) peak widths along the longitudinal direction are much broader than the instrumental resolution (Fig. 3), which means that the crystal coherence lengths are shorter than the value defined by the resolution presented above. The average crystal coherence length (ξ) is defined by $\xi = 1/\kappa$ (nm) according to Scherrer's equation, where κ (nm^{-1}) is the half width at half maximum of the (400) Bragg peak along the longitudinal direction in the reciprocal space. In the T phase, some peaks were resolution limited, where the crystal coherence lengths were more than 1 μm. To obtain information on the length scale of over 1 μm, we performed coherent x-ray scattering measurements [33,34]. By narrowing the incident beam to 10×10 μm^2, we obtained almost perfect spatial coherence of the x rays by considering the incident x-ray energy and the distance between the light source and the sample. Using the coherent x rays, a single sharp peak was observed at each measurement point along the x direction in the T phase. This suggests that the 10×10 μm^2 irradiated regions contain almost no faults. The typical size of domains in the T phase is estimated to be larger than 10 μm. The Ti composition dependence of the crystal coherence length is summarized in Fig. 2(d).

The crystal coherence length has a minimum near the M_B–M_C phase boundary and rapidly changes from approximately 70 nm to over 10 μm with the change in the Ti composition

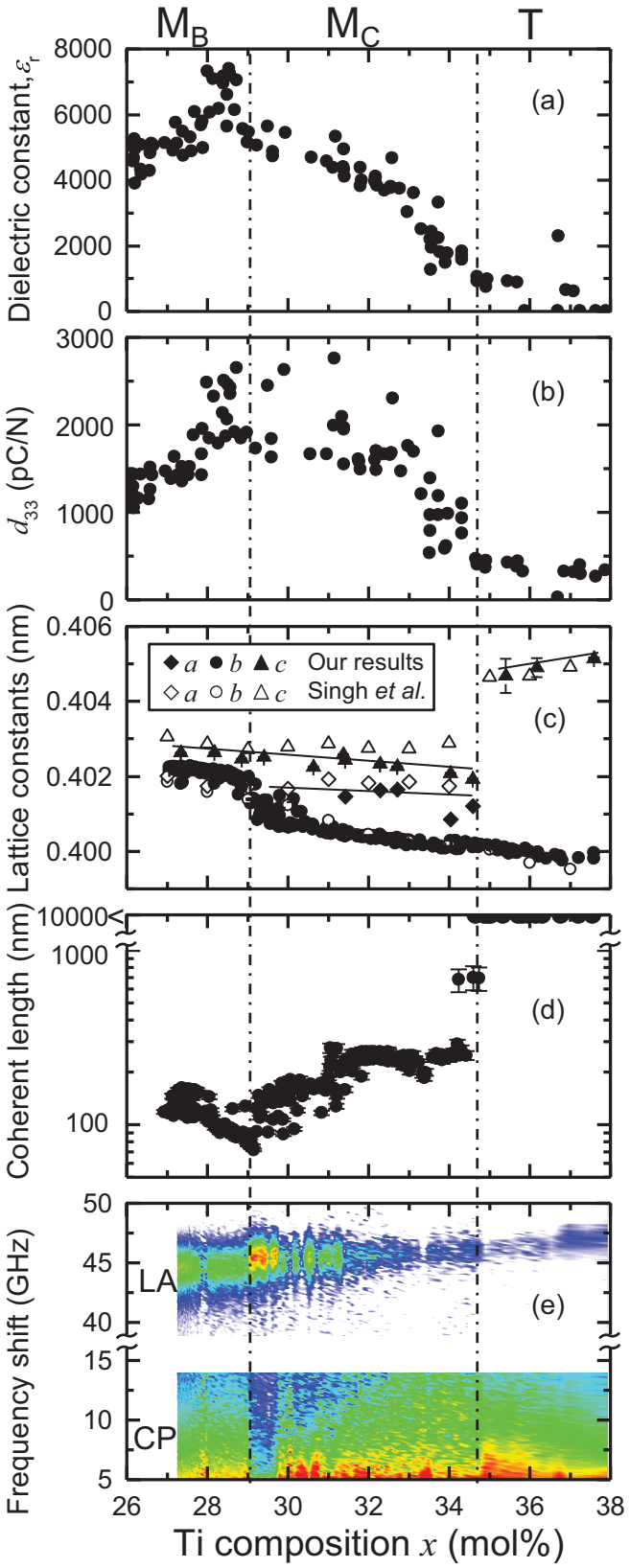

FIG. 2. (Color online) Ti composition dependence of (a) dielectric constant [11], (b) piezoelectric constant [11] (d_{33}), (c) lattice constants (solid marks are our results, open marks are previous results [28], solid lines are a guide to the eye), (d) crystal coherence length, and (e) contour maps of Brillouin spectrum.

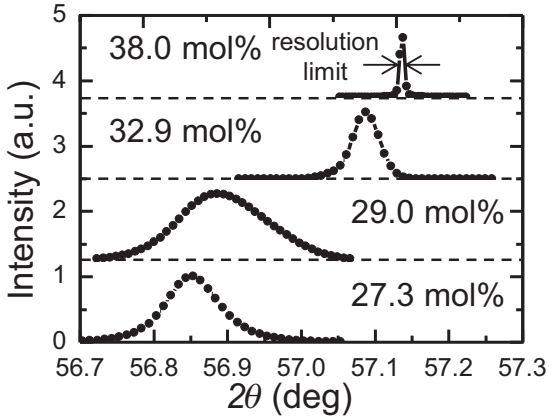

FIG. 3. (400) Bragg peak profiles measured along longitudinal direction at Ti compositions of 27.3, 29.0, 32.9, and 38.0 mol%. These profiles are normalized by the peak intensities.

of about 10 mol% in the crystal. The broadening trend of the Bragg peaks near the MPB was previously reported for PMN-xPT with coarse x steps (over 3 mol%) [35,36]. Our present results were obtained with fine x steps (0.04 mol%) and cover the two phase boundaries near the MPB along the x direction.

Figure 2(e) shows the intensity contour maps of the inelastic light scattering spectra of the longitudinal acoustic (LA) phonon mode and the central peak (CP) corresponding to the 40–50 GHz and the 0–15 GHz regions, respectively. The spectra are normalized by the total intensity of one spectrum of ±66.259 GHz except the ±5 GHz corresponding the Rayleigh scattering. Information on the polarization fluctuations can be obtained directly from the CP, and indirectly from the LA phonon mode via polarization-strain coupling [37,38]. The LA mode shows a hardening trend with increasing Ti composition, indicating that the crystal becomes stiffer with increasing Ti composition. This result can be understood from the volume reduction of the unit cell with increasing Ti composition [28,29]. The peak widths and relative intensities of the LA mode and CP show a clear change at the two phase boundaries determined by the x-ray diffraction, indicating that no clear difference can be seen between the bulk and the skin [25–27] region in this sample.

As mentioned in the introduction, a sharp peak of ε_r (~8000) can be seen at approximately 28.5 mol% [Figs. 2(a) and 2(b)]. This composition of 28.5 mol% corresponds to the M_B–M_C phase boundary observed at 29.0 mol% in Figs. 2(c) and 2(e), considering the error of ±0.6 mol%. ε_r gradually decreased between $x = 29$ and 34 mol%, and is almost completely suppressed above $x = 34.5$ mol% (in the T phase). d_{33} also shows similar behavior.

It is now clear that the crystal coherence length (ξ) at the sub-μm scale and the electrical response have a negative correlation over a wide Ti composition range. As shown in Fig. 2, the crystal coherence length decreases toward the M_B–M_C phase boundary, while the electrical response increases, with the former having a minimum and the latter having a maximum at the M_B–M_C phase boundary. The crystal coherence length increases from the M_B–M_C phase boundary towards the M_C–T phase boundary while the electrical response decreases, with

the former suddenly increasing and the latter decreasing at the M_C–T phase boundary. The evolution of the observed crystal coherence length with the Ti composition can explain the difference in the degree of electrical response between the M_B–M_C and M_C–T phase boundaries, shown in Figs. 2(a) and 2(b).

A similar negative correlation has been reported for $BaTiO_3$ with engineered domain configurations, where the smaller the domain size, the higher the degree of electrical response observed [39,40]. Domain-size effects have also been observed in PMN-xPT and $Pb(In_{1/2}Nb_{1/2})O_3$-PMN-PT with engineered domain configurations [41–43]. If the crystal coherence length corresponds to the domain size, the negative correlation near the MPB could be explained as a domain-size effect. As previously mentioned, the domain-size effects were observed in the compositionally uniform samples only by changing the external fields [39–42], whereas, in our case, the crystal coherence length was shown to be controlled by the Ti composition. Both cases can be understood as a domain-size effect, however, the mechanism of the domain-size control seen in the present Ti-composition-gradient sample remains to be solved.

A possible interpretation of the domain-size effect is that the electrical response of the domain walls is enhanced [39,40,44]. According to this interpretation, the electrical response of the bulk should strongly correlate with the volume of the domain walls. However, if we assume the domain-wall thickness to be equal to the lattice constant a, the value is reasonable in the case of normal ferroelectrics [45]. In the present case, the ratio of the volume of domain walls to the bulk is approximately a/ξ ($\sim$0.006 in the case of $\xi = 70$ nm), implying that the contribution of domain walls is too small to explain the present experimental results.

Recently, Iwata *et al.* have suggested that the effective domain-wall size under an electric field increases near the MPB. The regions of the metastable R (T) phase become the *thick* domain walls of the stable T (R) phase on the coexistence states [13,14]. This suggestion makes it worth considering the domain structures and susceptibility of the domain walls under an electric field. This should be clarified in future investigations of the relaxor ferroelectrics near the MPB.

Before closing this paper, it was found that the LA mode hardened by 0.6 GHz between 29.0 and 29.8 mol%, during which the intensities of the LA mode and CP increased and decreased, respectively, as shown in Fig. 2(e). Furthermore, the lattice constants gradually changed in the same region [Fig. 2(c)] despite the first-order phase transition. It will be interesting to clarify whether the O phase exists in this narrow region connecting the M_B and M_C phases because a transition from the M_B phase to the M_C phase without passing through the O phase is unnatural [6,28]. This should be studied carefully using our sample with a Ti composition gradient.

The phase diagram and the relationship between the crystal coherence length and the electrical response of PMN-xPT near the MPB have been precisely investigated using a single crystal with a Ti composition gradient by synchrotron x-ray diffraction and inelastic light scattering at room temperature. The crystal has two boundaries at Ti compositions of 29.0 and 34.7 mol%, which correspond to the phase boundaries between the M_B and M_C phases and between the M_C and T phases, respectively. The crystal coherence length determined by the widths of Bragg peaks varies by over two orders of magnitude in a 10 mol% range of the Ti composition. It was found that there is a strong negative correlation between the electrical response and the crystal coherence length at the sub-μm scale. We have confirmed that the results can be explained by the size effects of domains near the MPB.

ACKNOWLEDGMENTS

We would like to show our gratitude to the following people for light scattering experiments, samples, stimulating discussions, and comments: Dr. M. Matsushita (JFE-Mineral Co., Ltd.), Dr. T-H. Kim (Univ. of Tsukuba), Prof. H. Terauchi (Kwansei Gakuin Univ.), Prof. Y. Fujii (The Univ. of Tokyo), Prof. M. Iwata (Nagoya Inst. Tech.), the late Prof. K. Hirota (Osaka Univ.), and the late Dr. G. Shirane (Brookhaven Nat. Lab.). This work was partly supported by a MEXT Grant-in-Aid for Scientific Research on Priority Areas "Novel States of Matter Induced by Frustration" (Grant No. 19052002), JSPS Grants-in-Aid for Scientific Research for Young Scientists B (Grants No. 16740177 and No. 21710099), JSPS Grant-in-Aid for Scientific Research (C) (Grant No. 26400327). The synchrotron radiation experiments were performed at BL22XU of SPring-8 with the approval of Japan Synchrotron Radiation Research Institute (JASRI) (Proposals No. 2012A3713 and No. 2013A3713).

[1] T. R. Shrout and J. Fielding, Jr., in *Proceedings of the IEEE Ultrasonic Symposium, 1990* (IEEE, Piscataway, NJ, 1990), Vol. 2, pp. 711–720.
[2] B. Noheda, J. A. Gonzalo, L. E. Cross, R. Guo, S.-E. Park, D. E. Cox, and G. Shirane, Phys. Rev. B **61**, 8687 (2000).
[3] B. Noheda, D. E. Cox, G. Shirane, S.-E. Park, L. E. Cross, and Z. Zhong, Phys. Rev. Lett. **86**, 3891 (2001).
[4] B. Noheda, D. E. Cox, G. Shirane, J. Gao, and Z.-G. Ye, Phys. Rev. B **66**, 054104 (2002).
[5] K. Hirota, S. Wakimoto, and D. E. Cox, J. Phys. Soc. Jpn. **75**, 111006 (2006).
[6] D. Vanderbilt and M. H. Cohen, Phys. Rev. B **63**, 094108 (2001).
[7] H. Fu and R. E. Cohen, Nature (London) **403**, 281 (2000).
[8] K. Ohwada, K. Hirota, P. W. Rehrig, Y. Fujii, and G. Shirane, Phys. Rev. B **67**, 094111 (2003).
[9] Y. Ishibashi and M. Iwata, Japanese J. Appl. Phys. **37**, L985 (1998).
[10] Y. Ishibashi and M. Iwata, Japanese J. Appl. Phys. **38**, 800 (1999).
[11] M. Matsushita, Y. Tachi, and Y. Iwasaki, JFE Technical Report No. 8 (Japanese) (unpublished).
[12] S.-E. Park and T. R. Shrout, J. Appl. Phys. **82**, 1804 (1997).
[13] M. Iwata and Y. Ishibashi, Jpn. J. Appl. Phys. **52**, 09KF07 (2013).

[14] M. Iwata and Y. Ishibashi, Jpn. J. Appl. Phys. **51**, 09LE03 (2012).
[15] Y. M. Jin, Y. U. Wang, A. G. Khachaturyan, J. F. Li, and D. Viehland, Phys. Rev. Lett. **91**, 197601 (2003).
[16] Y. Tomita and T. Kato, J. Phys. Soc. Jpn. **82**, 063002 (2013).
[17] G. Xu, Z. Zhong, H. Hiraka, and G. Shirane, Phys. Rev. B **70**, 174109 (2004).
[18] M. Matsuura, K. Hirota, P. M. Gehring, Z.-G. Ye, W. Chen, and G. Shirane, Phys. Rev. B **74**, 144107 (2006).
[19] H. Luo, G. Xu, H. Xu, P. Wang, and Z. Yin, Jpn. J. Appl. Phys. **39**, 5581 (2000).
[20] F. Bai, J. Li, and D. Viehland, Appl. Phys. Lett. **85**, 2313 (2004).
[21] H. Okino, J. Sakamoto, and T. Yamamoto, Jpn. J. Appl. Phys. **42**, 6209 (2003).
[22] H. Wang, J. Zhu, N. Lu, A. A. Bokov, Z.-G. Ye, and X. W. Zhang, Appl. Phys. Lett. **89**, 042908 (2006).
[23] Y. Sato, T. Hirayama, and Y. Ikuhara, Appl. Phys. Lett. **100**, 172902 (2012).
[24] S. Bhattacharyya, J. R. Jinschek, H. Cao, Y. U. Wang, J. Li, and D. Viehland, Appl. Phys. Lett. **92**, 142904 (2008).
[25] G. Xu, H. Hiraka, G. Shirane, and K. Ohwada, Appl. Phys. Lett. **84**, 3975 (2004).
[26] G. Xu, P. M. Gehring, C. Stock, and K. Conlon, Phase Transitions **79**, 135 (2006).
[27] D. Phelan, E. Rodriguez, J. Gao, Y. Bing, Z.-G. Ye, Q. Huang, J. Wen, G. Xu, C. Stock, M. Matsuura, and P. Gehring, Phase Transitions **88**, 283 (2015).
[28] A. K. Singh and D. Pandey, Phys. Rev. B **67**, 064102 (2003).
[29] A. K. Singh, D. Pandey, and O. Zaharko, Phys. Rev. B **74**, 024101 (2006).
[30] K. Ikeuchi, K. Isawa, K. Yamada, T. Fukuda, J. Mizuki, S. Tsutsui, and A. Q. R. Baron, Jpn. J. Appl. Phys. **45**, 1594 (2006).
[31] T. Shobu, K. Tozawa, H. Shiwaku, H. Konishi, T. Inami, T. Harami, and J. Mizuki, AIP Conf. Proc. **879**, 902 (2007).
[32] S. M. Lindsay, M. W. Anderson, and J. R. Sandercock, Rev. Sci. Instrum. **52**, 1478 (1981).
[33] K. Ohwada, J. Mizuki, K. Namikawa, M. Matsushita, S. Shimomura, H. Nakao, and K. Hirota, Phys. Rev. B **83**, 224115 (2011).
[34] K. Ohwada, J. Mizuki, M. Matsushita, and K. Namikawa, Phys. Rev. B **90**, 104109 (2014).
[35] A. Kania, E. Talik, M. Kruczek, and A. Slodczyk, J. Phys.: Condens. Matter **17**, 6737 (2005).
[36] G. Xu, D. Viehland, J. F. Li, P. M. Gehring, and G. Shirane, Phys. Rev. B **68**, 212410 (2003).
[37] S. Tsukada and S. Kojima, Phys. Rev. B **78**, 144106 (2008).
[38] S. Tsukada, Y. Hidaka, S. Kojima, A. A. Bokov, and Z.-G. Ye, Phys. Rev. B **87**, 014101 (2013).
[39] S. Wada, K. Yako, H. Kakemoto, T. Tsurumi, and T. Kiguchi, J. Appl. Phys. **98**, 014109 (2005).
[40] S. Wada, T. Muraishi, K. Yokoh, K. Yako, H. Kamemoto, and T. Tsurumi, Ferroelectrics **355**, 37 (2007).
[41] D. Lin, H. J. Lee, S. Zhang, F. Li, Z. Li, Z. Xu, and T. R. Shrout, Scr. Mater. **64**, 1149 (2011).
[42] Z.-Y. Shen, Y. Tang, S. Zhang, J. Luo, Y. Li, and T. R. Shrout, Scr. Mater. **72-73**, 17 (2014).
[43] D. Lin, S. Zhang, Z. Li, F. Li, Z. Xu, S. Wada, J. Luo, and T. R. Shrout, J. Appl. Phys. **110**, 084110 (2011).
[44] R. Ahluwalia, T. Lookman, A. Saxena, and W. Cao, Phys. Rev. B **72**, 014112 (2005).
[45] H. Odagawa and Y. Cho, Japanese J. Appl. Phys. **39**, 5719 (2000).